2011

Simulating the time-dependent diffusion coefficient in mixed-pore-size materials

Zhigang Zhang
University of Rhode Island

David L. Johnson

Lawrence M. Schwartz

Simulating the time-dependent diffusion coefficient in mixed-pore-size materials

Terms of Use

Simulating the time-dependent diffusion coefficient in mixed-pore-size materials

Zhigang Zhang,[1,2] David L. Johnson,[1] and Lawrence M. Schwartz[1,3]

[1]*Schlumberger Doll Research, One Hampshire Street, Cambridge, Massachusetts 02139, USA*
[2]*Graduate School of Oceanography, University of Rhode Island, Kingston, Rhode Island 02881, USA*
[3]*Department of Earth, Atmospheric and Planetary Sciences, Massachusetts Institute of Technology, Cambridge, Massachusetts 02139, USA*

Porous media with a wide distribution of pore sizes are quite common. We show that variable-step-size random walk simulations can be used to model the time-dependent diffusion coefficient $D(t)$ in such porous media. The issue to be overcome is that, in variable-step-size walks, each walker carries its own "clock," and its position is known only at a random set of times. Thus, a direct ensemble-average calculation of $\langle \Delta r^2(t) \rangle$ (the mean-square distance traveled at time t) is problematic. We introduce a sequence of approximations that overcome this apparent difficulty. Calculations are carried out on periodic systems that contain pores of quite different sizes. Where possible, our results are compared to those obtained using fixed-step-size random walks.

I. INTRODUCTION

Liquid-saturated porous media arise in a number of contexts, viz., polymer gels, catalytic beds, granular materials, and sedimentary rocks. If a single liquid fills the pore space we have a two-component composite; in three dimensions both components form percolating channels through the system. Typically, in a liquid, the mean free path between molecular collisions is much smaller than the physical dimensions of the pore space. In this case molecular diffusion is of interest as an indirect probe of the system's structure and transport properties [1–10].

There are many contexts in which one might study the time dependence of diffusion in disordered systems. For example, if the geometry of the material is changing due to external forces or internal reactions, then the effective diffusion characteristics will evolve with time. In the present paper, however, we consider porous media whose structure is fixed. We picture an initially uniform distribution of particles released in the pore space and undergoing diffusion that is hindered by collisions with the solid phase. (We do not consider absorbtion of diffusing particles at the solid interface [11,12]; all of the results presented here are easily generalized to treat this possibility.) In this context, a time-dependent diffusion coefficient $D(t)$ reflects the fact that diffusion is different depending on how much time the diffusing particles have had to explore the pore space. $D(t)$ can be measured directly by pulsed field gradient spin-echo experiments [3–5,7]. In these experiments the magnitude, direction, and temporal spacing of the applied gradient pulses define a wave-vector- (**k**-) and time-(*t*-) dependent magnetization $M(\mathbf{k},t)$. In isotropic systems this quantity depends only on the magnitude of **k**, and the definition of the time-dependent diffusion coefficient is

$$-\lim_{k \to 0} \frac{\partial \ln[M(k,t)]}{\partial k^2} = \frac{\langle r^2(t) \rangle}{6} \equiv D(t)t. \quad (1)$$

(More generally, the diffusion coefficient is a symmetric 3×3 tensor.) The behavior of $D(t)$ at short times is directly related to an important geometrical parameter, the surface to volume ratio of the pore space, S/V_p [4]. The long-time limit of $D(t)$ is simply, and exactly, related to electrical conduction through the pore network [1,2,5]. The short- and long-time behaviors of $D(t)$ are summarized in Eqs. (5) and (6) below.

In simple porous media the spectrum of pore sizes is relatively narrow. In such systems the behavior of $D(t)$ can be modeled using techniques based on *fixed-step-size* random walks; one simply needs to choose the step size to be small compared to the diameter of the throats connecting adjacent pores. However, in many cases of interest (and of practical importance) there is a wide range of pores sizes [13–15]. In this case random walks that employ a fixed step size are impractical; if the step size is small compared to the smallest throat diameters, the walker's progress through the largest pores will be very inefficient. What about methods based on variable-step-size random walks, for example, first-passage techniques [1,2,16–18]? It might appear that these methods are also not well suited to calculating $D(t)$. In variable-step-size walks, each walker carries its own "clock"; the clock advances by a large amount when the walker takes a big step and by a small amount when the walker takes a small step. However, to calculate $D(t)$ we have to be able to *interrogate* each walker at a specified array of times $\{T_k\}$. Because the clocks carried by different walkers are not synchronized with the interrogation times, walkers will, in effect, step over these times, and information about where the walker was at time $t = T_k$ will be lost.

Our objective in this paper is to show that variable-step-size methods can, in fact, be adapted to the calculation of $D(t)$. In Sec. II we will introduce a sequence of three approximations, all based on variable-step-size random walks. These approximations allow us to calculate $D(t)$ accurately and efficiently. We illustrate our techniques with calculations based on a simple ordered packing of (possibly) overlapping spherical grains. This model has pores of a single size so we can compare our approximations to accurate fixed-step-size random walk calculations. In Sec. III we introduce models that have bimodal pore size distributions. These models are again based on periodic grain packings, and the mismatch in pore sizes can be set to any desired value. Here we find that our approximate calculations yield good results over the entire range of times studied. In the short-time regime we can compare our approximations to direct fixed-step-size calculations and the agreement is excellent. In Sec. IV we

present our conclusions and describe related future research directions.

II. SIMULATING DIFFUSION WITH VARIABLE-STEP-SIZE RANDOM WALKS

The context in which we are doing these random walk simulations is the continuum diffusion equation for molecules of a liquid confined to a porous solid. Here, the mean free path for molecule-molecule collisions is orders of magnitude smaller than the smallest feature in the porous medium, so we take it to be zero. The relevant Green's function is defined by the solution to the continuum diffusion equation

$$D_0 \nabla^2 G(\mathbf{r},\mathbf{r}_0,t) - \frac{\partial G(\mathbf{r},\mathbf{r}_0,t)}{\partial t} = 0, \qquad (2)$$

subject to the boundary condition on the pore-grain interface Σ,

$$[D_0 \hat{\mathbf{n}} \cdot \boldsymbol{\nabla} G(\mathbf{r},\mathbf{r}_0,t) + \rho G(\mathbf{r},\mathbf{r}_0,t)] \mid_{\mathbf{r} \in \Sigma} = 0, \qquad (3)$$

with initial condition $G(\mathbf{r},\mathbf{r}_0,t=0) = \delta(\mathbf{r} - \mathbf{r}_0)$. Here, D_0 is the diffusion constant in the unbounded liquid. ρ is the surface relaxivity; it describes the increased decay rate for molecules at the surface Σ. Mitra *et al.* [4] describe how one may compute the quantity $M(k,t)$, and thereby $D(t)$ [Eq. (1)], from the solution to Eqs. (2) and (3). $M(k,t)$ and $D(t)$ are measurable with standard nuclear magnetic resonance techniques.

In the present paper we specify to the case when there is no surface relaxivity, $\rho \equiv 0$, although our technique can be generalized to cases when $\rho \neq 0$. Our approach is to use random walkers to deduce the relevant statistics for $\langle r^2(t) \rangle$ implied by the solution to Eqs. (2) and (3).

In principle, once the geometry of the pore space is defined, we can always simulate diffusion with a fixed-step-size random walk. Walkers are placed at random in the pore space; they take steps of a fixed size ϵ, and the clock advances by $\Delta t = \epsilon^2/(6D_0)$, which is the exact result implied by the diffusion equation. After a specified number of time steps, each walker is asked the distance r it has traveled from its starting point. For example, If we interrogate every ten steps then $\{T_k\} = 10k\epsilon^2/(6D_0)$. The times T_k need not be evenly spaced; what is important is that, at each time T_k, *all* the walkers contribute to the average of $r^2(T_k)$.

What happens when a walker hits a grain? The boundary conditions on the diffusion equation call for zero current into the solid phase [19]. This translates to having the walker undergo specular reflection at the boundary; the distance traveled is still ϵ [20] and the clock advances by $\epsilon^2/(6D_0)$ with each step. This algorithm can be somewhat complicated to implement because direct specular reflection may put the walker back into the solid phase (for example if we are near a sharp corner of the pore space).

It is possible to deduce meaningful results for the long-time behavior of $D(t)$ using, e.g., diffuse reflectivity at a surface [6], but we employ the specular condition so as to guarantee the validity for short times of Eq. (5) (below), which was derived under the assumption of specular reflection at an internal surface [4]. The easiest way to see that this implies specular reflection is to note that when the walker is near enough the

pore-grain interface appears to be flat. In this case the exact solution to Eqs. (2) and (3) is

$$G(\mathbf{r},\mathbf{r}_0,t) = G_0(\mathbf{r},\mathbf{r}_0,t) + G_0(\mathbf{r},\mathbf{r}_M,t), \qquad (4)$$

where G_0 is the Green's function for an unbounded liquid and $\mathbf{r}_M \equiv [x_0,y_0, -z_0]$ is the image of the initial walker at $\mathbf{r}_0$, mirrored through the surface of solid, taken to be the xy plane. Our random walker rule is that any walker attempting to take a step from position $\mathbf{r}_0$ into the grain space is removed and replaced by the mirror image trajectory starting at $\mathbf{r}_M$, and ending up in the pore space, i.e., a specular reflection. Equation (23) of Mitra *et al.* [4] is the Laplace transform of our Eq. (4).

As noted above, if the pore dimensions vary widely, fixed-step-size random walks are not practical and we have to employ variable-step-size techniques. The most straightforward of these is based on the first-passage algorithm [1,2,6,11–13]. Each step begins by determining the radius R of the largest sphere that can be drawn around the walker's current position that does not intersect the solid phase. The walker then jumps to a random point on the surface of that sphere and the clock advances by $\Delta t = R^2/(6D_0)$. From that position we again determine the radius of the largest inscribed sphere and continue the process. This algorithm allows the walker to move efficiently through large regions of the pore space. When the walker gets to within a prescribed distance δR of the solid interface the algorithm changes and we revert to a walk with a fixed step size. There the step length ϵ is chosen to be small compared to the narrowest throats in the pore network [21] and, typically, we take $\delta R = 2\epsilon$. After a certain number of fixed-length steps and a certain number of collisions with the solid phase, the walker will leave the layer of width δR and the stepping algorithm goes back to steps based on the construction of maximal inscribed spheres.

In the variable-step-size process we have just described, each walker has a known position $\mathbf{r}_n$ and known "clock times" t_n after completing the nth step in the sequence. However, these clock times are different for each walker and, in general, are not related to the interrogation times T_k. Because the pore sizes vary widely, it is convenient to arrange the times $\{T_k\}$ in a logarithmic sequence (e.g., 0.01,0.03,0.06,0.10,0.30,0.60,1.0,...). Let us suggest a simple way to construct the average $\langle r^2(T_k) \rangle$ which we refer to as the *back-up* approximation. Suppose that in taking a step from $\{\mathbf{r}_n,t_n\}$ to $\{\mathbf{r}_{n+1},t_{n+1}\}$ the walker looks at its clock and discovers that it has crossed over one or more of the interrogation times, beginning with T_l. The walker simply backs up to the point $\mathbf{r}_n$ and takes a step of length $R = [6D_0(T_l - t_n)]^{1/2}$. This step advances its clock to $t_{n+1} = T_l$ and we can then register the walker's position at the time T_l. The walker then continues the variable-step-size walk, always checking its clock relative to the sequence of times T_k. It might seem that this process offers little gain in efficiency (compared to a fixed-step walk) since the walker will often have to back up after talking a large step. However, because the times T_k are arranged in a logarithmic scale, it is only the first few steps in each walker's sequence that are materially slowed down.

We can test these ideas on the grain consolidation (GC) model [22]. In Fig. 1 we show a periodic arrangement of
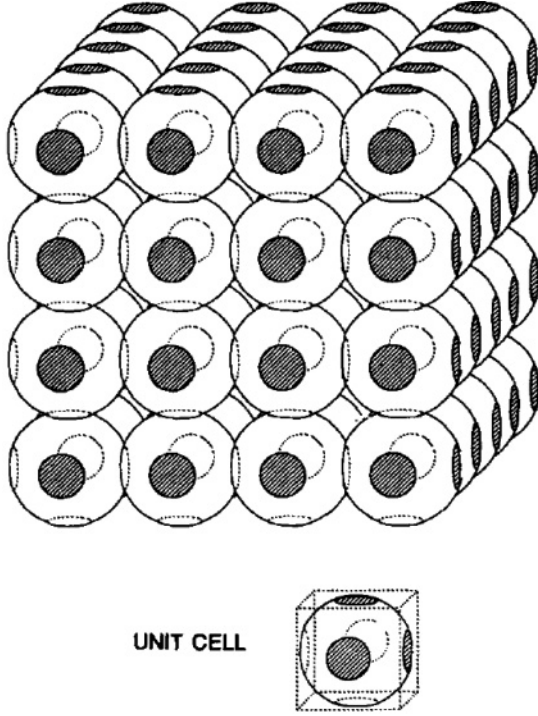
FIG. 1. Simple cubic grain consolidation (GC) model. Overlapping spherical grains are arranged on a cubic lattice with lattice constant $a = 200$ μm.
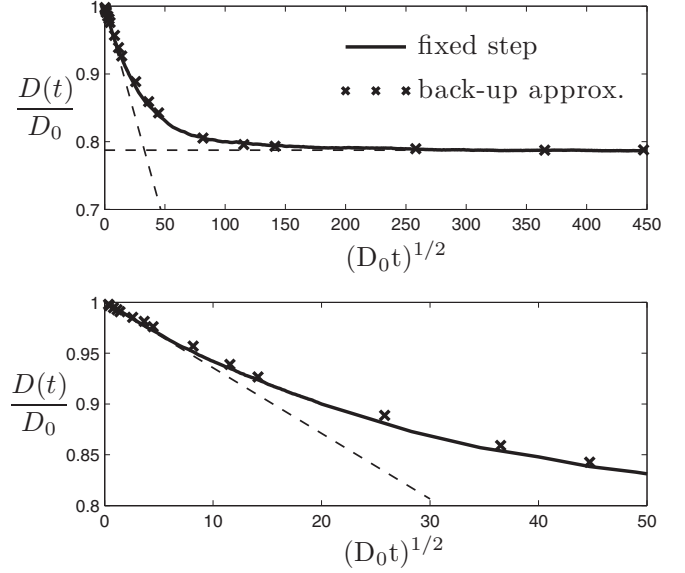

FIG. 2. Comparison of calculated $D(t)$ values for simulations based on fixed-step-size random walks (solid curves) and first-passage walks combined with the back-up approximation (crosses). The sphere radius in the GC model is $R = 95$ μm and the porosity $\phi = 0.551$. The dashed curves correspond to the limits described in Eqs. (5) (which can be derived analytically) and (6) (taken from the calculations of [23]). In the upper panel results are shown over a wide range of times; in the lower panel the short-time behaviors of the two simulations are compared in more detail.

spherical grains on a simple cubic lattice. The grains are pictured as consolidated (i.e., overlapping) but they will not be so if the grain radius is taken to be less than half the length of the unit cell edge. In Fig. 2 we compare the results of fixed-step -size random walks with those based on the back-up approximation. In the fixed-step-size calculations $\epsilon = 1$ μm ($= 0.005 \times$ the 200 μm cube edge). The same value of ϵ is employed in the back-up simulation when the walker is in the δR layer around each grain. In this sense the calculations can be said to resolve the structure of the pore geometry equally. In general, the agreement is excellent although, at short to intermediate times, the back-up results differ slightly from the fixed-step data. The dashed lines in these figures represent the exact results for short and long times:

$$\lim_{t \to 0} D(t) = D_0 \left[1 - \frac{4}{9\sqrt{\pi}} \frac{S}{V_p} (D_0 t)^{1/2} + \cdots \right], \quad (5)$$

$$\lim_{t \to \infty} D(t) = \lim_{t \to \infty} \frac{\langle r^2 \rangle}{6t} = \frac{D_0}{\phi F}. \quad (6)$$

Here S is the pore surface area, V_p is the pore volume, and F is the electrical formation factor. Equation (5) was derived under the specific assumption that the diffusing entities undergo specular reflection at an internal wall [4], which is why we employ the specular condition in our simulations. Equation (6) is essentially the Einstein relation between diffusion and electrical conductivity [1,5].

That the back-up approximation yields reasonable results is not surprising; we have simply adjusted the step length so that each walker finishes a step at every interrogation time. We can now suggest two additional approximations that are simpler and slightly more efficient than the back-up approximation.

Suppose that in going from the nth to the $(n + 1)$th step, the walker discovers that it has passed over one or more interrogation times. (Typically, if the walker starts within a relatively open region of the pore space, its first step will pass over several of the T_k.) We certainly do not know what path the walker took in going from $\mathbf{r}(t_n)$ to the point $\mathbf{r}(t_{n+1})$. Within the first-passage framework, $\mathbf{r}(t_{n+1})$ lies on the surface of the largest sphere centered at $\mathbf{r}(t_n)$ that does not intersect the solid grains, and we assume that, in going from $\mathbf{r}(t_n)$ to $\mathbf{r}(t_{n+1})$, the walker has been confined to the interior of this sphere. If an ensemble of walkers went between these two points, their average position at any time between t_n and t_{n+1} would lie on the line connecting $\mathbf{r}_n$ to $\mathbf{r}_{n+1}$. Alternatively, if the same direction cosines were used to define the walker's position at an earlier time, it would find itself on that same line. With this in mind, we suggest the following interpolation formula to assign the walker a position on that line at each of the intermediate times T_k:

$$\mathbf{r}(T_k) = \mathbf{r}(t_n) + [\mathbf{r}(t_{n+1}) - \mathbf{r}(t_n)] \left[\frac{T_k - t_n}{t_{n+1} - t_n} \right]^{1/2}, \quad (7)$$

where $t_n \leqslant T_k \leqslant t_{n+1}$. This $t^{1/2}$ interpolation allows us to take full advantage of the variable-step-size random walk. In contrast to the back-up approximation, here we never have to revert to smaller steps in order to update our data at each interrogation time. While Eq. (7) does require us to calculate several corrected positions, these intermediate positions do not have to be tested to see if the walker has hit a grain. This will be especially important in the microporous systems discussed in Sec. III. With as many as 10^5 grains in each unit cell, the

majority of the computational overhead lies in testing each location. As noted above, this issue is most important for the walker's first few steps.

The other algorithm we employ for the purpose of acquiring random walk statistics avoids completely the need for saying where the particle is located at intermediate times, but simply keeps track of its mean square displacement from $\mathbf{r}(t_n)$. Let us consider the random walk statistics of those particles which are at some position $\mathbf{r}$ at time t_n and will eventually end up on the surface of the first-passage sphere at $\mathbf{r}(t_{n+1})$. Given the assumption that the walker undergoes free diffusion between t_n and t_{n+1}, we have for the intermediate time T_k

$$\langle \Delta r^2 \rangle = 6D_0(T_k - t_n). \tag{8}$$

More generally, we write

$$\mathbf{r}(T_k) = \mathbf{r}(t_n) + \Delta\mathbf{r}(T_k - t_n), \tag{9}$$

and so

$$\langle r^2(T_k) \rangle = r^2(t_n) + 2\mathbf{r}(t_n) \cdot \langle \Delta\mathbf{r}(T_k - t_n) \rangle + \langle | \Delta\mathbf{r}(T_k - t_n) |^2 \rangle. \tag{10}$$

Because the walkers' diffusive motion is uncorrelated with its starting point $\mathbf{r}(t_n)$, the cross term in Eq. (10) vanishes and, from (8), the third term is simply equal to $6D_0(T_k - t_n)$. We are now able to build statistics for the random walkers at the intermediate times for these walkers according to the rule

$$\langle r^2(T_k) \rangle = r^2(t_n) + 6D_0(T_k - t_n). \tag{11}$$

With this algorithm, we simply bin $\langle r^2(T_k) \rangle$ values for each intermediate time T_k according to Eq. (11); the question of where the particle actually is located at intermediate times never arises. We refer to Eq. (11) as the $\langle \Delta r^2 \rangle$ interpolation and note that the algorithm given by Eq. (7) automatically satisfies Eq. (11).

In Fig. 3 calculated results based on the $\langle \Delta r^2 \rangle$ approximation and the $t^{1/2}$ interpolation are compared for the same model considered in Fig. 2. As expected, these two approximations yield identical results and are both in good agreement with the fixed-step-size data. In Fig. 4 we apply the back-up and $t^{1/2}$ approximations to a version of the model described in Fig. 1 with overlapping spherical grains, and the porosity is reduced to $\phi \approx 0.202$. In this system the tortuosity is increased (i.e., diffusion from pore to pore is more difficult) but, again, we see that our approximate calculations compare well with the fixed-step data.

The results presented here describe three-dimensional porous media. It is clear that the algorithms we are proposing are valid in any number of spatial dimensions. Of course, the detailed form of Eqs. (1), (5), (8), and (11) is correct only in three dimensions.

III. SYSTEMS WITH BIMODAL PORE SIZE DISTRIBUTIONS

In Figs. 5, 6, and 7 we introduce three periodic models in which the pores have a bimodal size distribution. First is the micro-grain consolidation (μ-GC) model (Fig. 5). Here the originally solid grains are now microporous; they are comprised of smaller (possibly) overlapping grains centered
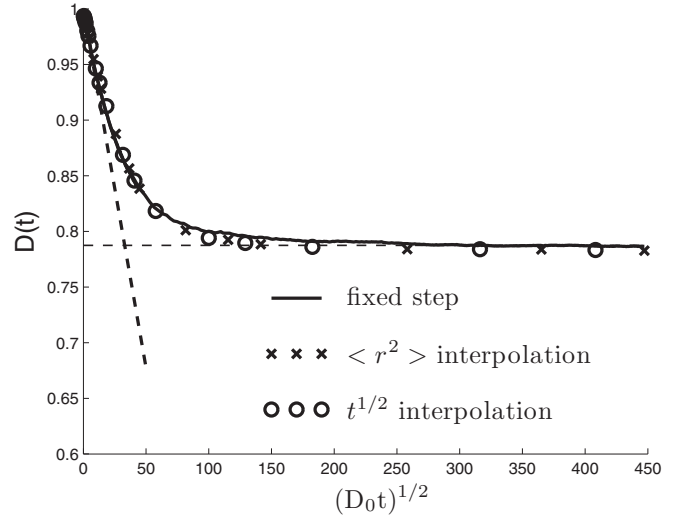

FIG. 3. Comparison of calculated $D(t)$ values for simulations based on fixed-step-size random walks (solid curves) and first-passage walks combined with the $\langle \Delta r^2(t) \rangle$ approximation, Eq. (11), and the $t^{1/2}$ interpolation, Eq. (7). The underlying model is the same as in Fig. 2.

on a lattice constructed by dividing the original unit cell into smaller cells. The scale factor governing this division controls the degree of mismatch in the model's pore sizes. As in Fig. 1, we take the edge of the large cube to be 200 μm; scale factors of 20 and 50 then correspond to smaller cells with edge lengths of 10 and 4 μm, respectively. If the original grains overlap, the μ-GC model has pathways through the large open pores and (roughly) parallel pathways through the micro-porous grains. In Figs. 6 and 7 we have two models in which the pathways through the system involve (roughly) series connections of the macro- and microporosity. In the embedded spherical pore (ESP) model (Fig. 6) we have nonoverlapping spherical pores embedded in a microporous
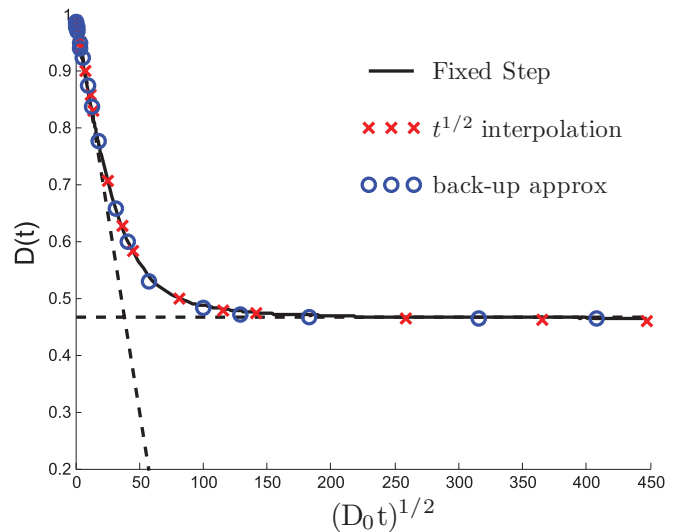

FIG. 4. (Color online) Fixed-step-size calculations of $D(t)$ compared with the back-up approximation and the $t^{1/2}$ interpolation, Eq. (7). The sphere radius in the GC model is $R = 120$ μm and the porosity $\phi = 0.202$.
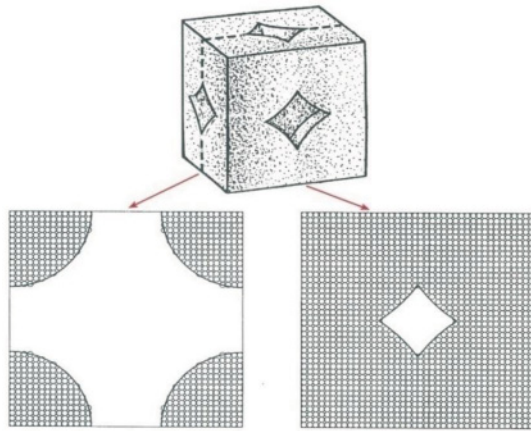
FIG. 5. (Color online) A microporous version of the GC model in which the (formerly solid) grains are comprised of smaller grains whose centers lie on a lattice constructed by subdividing the original unit cell by a scale factor.

background. Again, a scale factor controls the size of the lattice on which the micrograins are centered. In the channel model (Fig. 7) the spherical macropores are connected by channels that are filled with microporous grains. While these three models are certainly idealized, they capture some of the features found in detailed studies of the three-dimensional microstructure of many carbonate rocks [13–15]. Finally, in applying the algorithms developed in Sec. II to these models, one must check that the smallest regions of the pore space are still very large compared to molecular mean free paths in the pore fluid.

In Fig. 8 we compare short-time data for calculations based on fixed-step-size random walks and the $t^{1/2}$ interpolation applied to the μ-GC model depicted in Fig. 5. (We could just as easily have employed the back-up or $\langle \Delta r^2 \rangle$ approximations in this comparison; as before, the three approximations yield
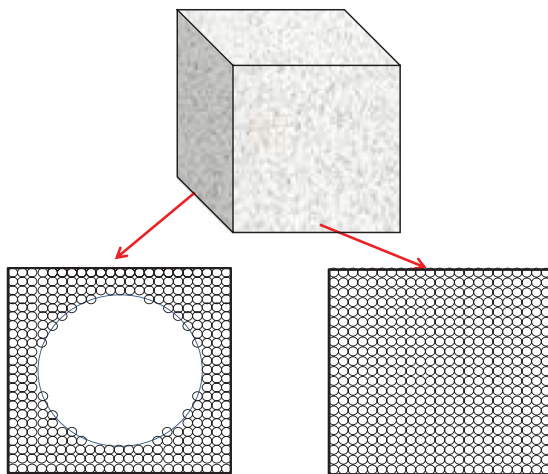

FIG. 6. (Color online) The embedded spherical pore (ESP) model in which a cubic array of large spherical pores is surrounded by smaller overlapping spheres arranged on a lattice commensurate with the larger lattice (as in the μ-GC model). Because the radii of large and small grains are independent, the amounts of macro- and microporosity can be varied independently.
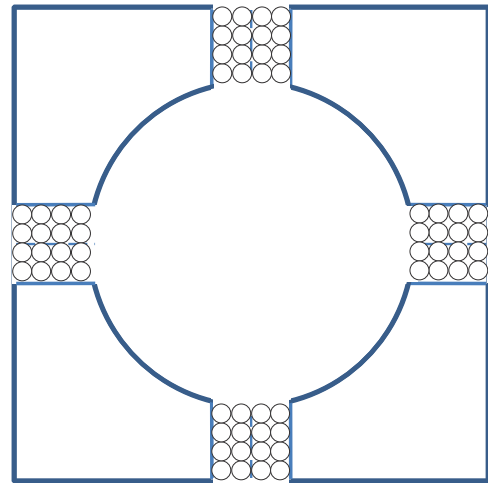

FIG. 7. (Color online) The channel model in which large spherical pores in a cubic array are connected by channels containing small grains.

essentially identical results.) Two values (20 and 50) are taken for the scale factor used to construct the cells containing the micrograins. In both cases, the total porosity is $\phi = 0.26$; the macro- and micropore volume fractions are 0.175 and 0.085, respectively. The value of ϵ used in the fixed step calculations is $0.005\times$ the edge length of the small cubic cells; this is directly analogous to the choice made in connection with Figs. 2–4. The same value of ϵ is employed in the layer of width δR around each micrograin in the $t^{1/2}$ interpolation. In this sense the resolution of the two calculations is the same. We see that the $t^{1/2}$ interpolation is in good agreement with the fixed-step-size results. Recalling Eq. (2), the short-time behavior of $D(t)$ is controlled by the ratio S/V_p. By design, the two models considered here have the same value for V_p but very different values for S. We see that the initial decrease of $D(t)$ becomes more pronounced when the scale factor is increased from 20 to 50.
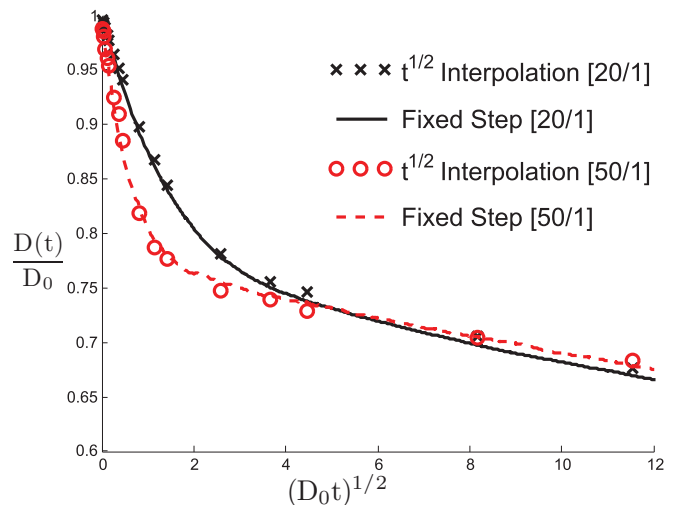

FIG. 8. (Color online) For the μ-GC model (Fig. 5), short-time results based on fixed-step-size random walk calculations compared with results obtained from the $t^{1/2}$ interpolation. Results are shown for two choices of the macro-micro scale factor.

TABLE I. CPU times (in seconds) for simulations based on fixed-step-size random walks, the back-up approximation, and the $t^{1/2}$ interpolation. The calculations were carried out on a Sun Fire v490 with four 150 MHz SPARC IV + processors and 16 Gbytes of RAM. They are based on the μ-GC model for two choices of the scale factor (as in Figs. 8–10). (As noted in the text, the value of ϵ used in the fixed-step calculations equals the minimum step size in the two variable-step-size simulations.) All the numbers represent an average over three runs, each with 200 walkers. The saving in CPU time in going from the back-up approximation to the $t^{1/2}$ interpolation is roughly 7.5%. [Additional calculations (not shown) indicate that the difference between the $t^{1/2}$ and $\langle \Delta r^2 \rangle$ interpolations is less than 0.5%.] As expected, for each approach, CPU times increase in direct proportion to the number of walkers.

		CPU comparison	
$D_0 t_{max}$	Algorithm	20/1	50/1
200 μm2	Fixed step size	1315.40	8023.6
	Back-up approx.	37.9	212.6
	$t^{1/2}$ interpolation	35.1	197.7
1000 μm2	Fixed step size	6667.4	40957.5
	Back-up approx.	198.1	1079.2
	$t^{1/2}$ interpolation	184.2	1005.6

We emphasize that extending the fixed-step-size results in Fig. 8 to long times would be quite inefficient from a computational viewpoint. In Table I we compare CPU times for calculations based on fixed-step-size random walks, the back-up approximation, and the $t^{1/2}$ interpolation. These data cover only relatively short times compared to the calculations presented in Fig. 9 (below). In addition, the results in Fig. 9 are based on an average over at least 100 000 walkers compared to the 200 walkers employed in Table I. We note, first, that the two variable-step-size methods provide a reduction in
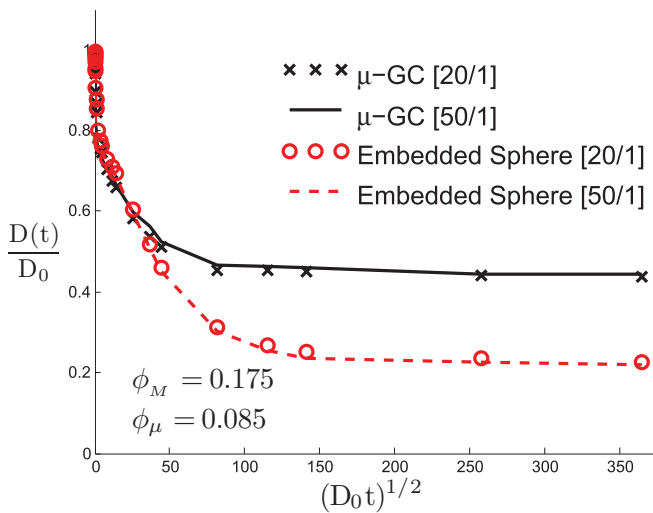

FIG. 9. (Color online) Calculated values of $D(t)$ for long times compared for four representations of the mixed pore size models shown in Figs. 5 and 6. The calculations are based on the $t^{1/2}$ interpolation. All four models are arranged to have the same fractions of macro- and microporosity. The two models with scale factor 20 have the same surface area (as do the models with the scale factor 50).
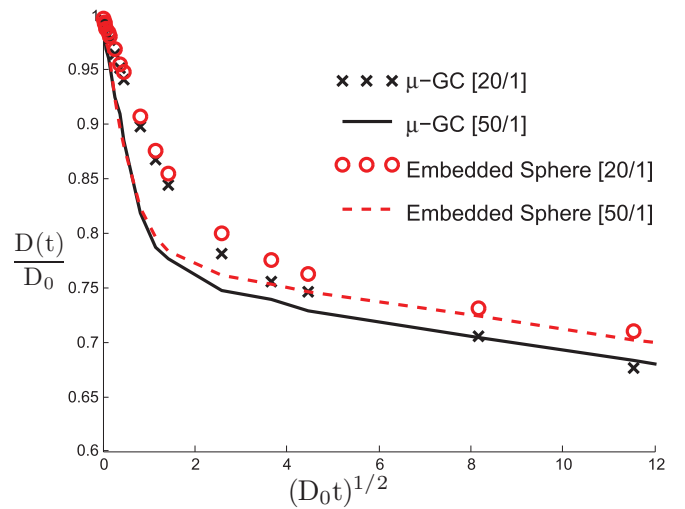

FIG. 10. (Color online) Comparison of calculated values of $D(t)$ for short times for the same models described in Fig. 9. The calculations are based on the $t^{1/2}$ interpolation.

CPU time between 35 and 40 compared to the fixed-step-size calculations. Second, the $t^{1/2}$ interpolation is seen to be roughly 7% faster than the back-up approximation. While CPU time is directly proportional to the number of walkers, we believe that the factor of 35–40 gain in computing speed seen here would only grow if the calculations were extended to times that were longer by a factor of 100 because of the overhead associated with the number of actual steps required by the fixed-step-size method.

In Figs. 9 and 10 we examine results based on the $t^{1/2}$ interpolation applied to the μ-GC and ESP models. The parameters in both models are adjusted to give the same macro- and micropore fractions, 0.175 and 0.085, as in Fig. 8. Again, for each model we present results for two values of the scale factor. At long times (Fig. 9) the calculated results are controlled by whether or not there are connected pathways through the (highly conducting) macropores. If the long-range pathways must go through (more resistive) micropores, then the effective diffusion coefficient will be significantly reduced. At short times (Fig. 10) the behavior of $D(t)$ is again controlled by the surface area S, and the precise nature of the long-range pore space connections is of no importance.

In Fig. 9 we see that the long-time behavior of $D(t)$ is independent of the scale factor. This is expected because the effective conductivity of the microporous regions depends on their porosity but does not depend on the absolute size of the pores and grains. (Changing the scale factor does not affect the porosity within the microporous regions.)

We conclude this discussion with Fig. 11 in which we consider results based on the model shown in Fig. 7. We compare two systems; in the first the channels connecting the spherical macropores are empty and in the second they are filled with consolidated micrograins. For the parameters we have chosen, the difference in porosity between these two systems is not large, $\phi = 0.177$ vs $\phi = 0.155$. We see, however, that the difference in $D(t)$ at long times is quite marked. When the channels are filled with micrograins, the long-range pathways are distinctly more tortuous. In
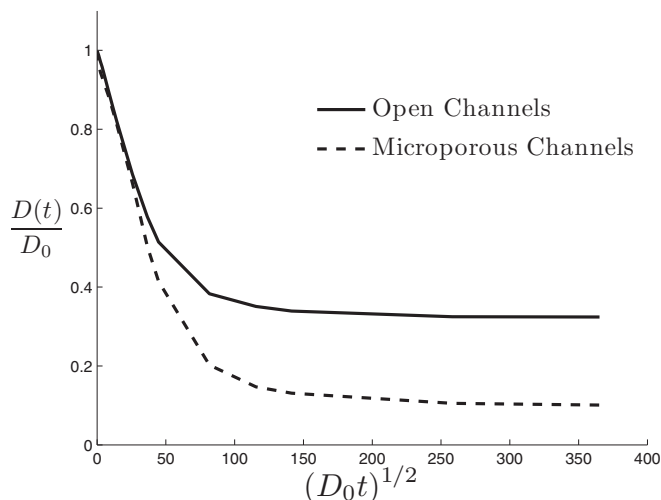
FIG. 11. Comparison of calculated values of $D(t)$ for two representations of the channel model (Fig. 7). The calculations are based on the $t^{1/2}$ interpolation. When the channels connecting the large pore are filled with small grains, the scale factor equals 40.

these calculations the scale factor equals 40. Changing this value (while leaving the other parameters fixed) will affect the short-time behavior of $D(t)$ while leaving the porosity and the long-time results for $D(t)$ essentially unchanged.

IV. CONCLUSIONS AND FUTURE DIRECTIONS

We have shown that any of three different approximations can be used to calculate the time-dependent diffusion coefficient $D(t)$ in systems with a wide range of pore sizes. Our illustrative calculations involved relatively simple periodic systems with a bimodal pore size distribution. However, these results can be extended to other model porous systems, for example, models constructed from three-dimensional x-ray microtomography [9,14,17,24,25]. All that is required to apply the algorithms we have described is to be able to determine the distance to the closest grain from any point on the pore space.

In a future paper, we will compare the present simulations with results based on direct numerical calculations of the eigenvalues and eigenfunctions for the diffusion equation. As long as the value of the scale factor in our models is no greater than about 20, finite-difference techniques are quite efficient and yield results for $D(t)$ that are very close to those obtained here [30,31]. The methods presented in this paper can also be employed to describe diffusion and relaxation in complex porous media [9,13,14]. Of particular interest is the possibility of simulating two- and three-dimensional magnetic resonance experiments [26–29]. These measurements, often referred to as T_1-T_2 and T_2-T_1-T_2 correlations, attempt to isolate cases in which diffusion carries particles from pore to pore. The models and techniques we have developed are well suited to describing this phenomenon [13] and we hope to address some of the (as yet) unresolved issues.

[1] I. C. Kim and S. Torquato, J. Appl. Phys. **68**, 3892 (1990).

[2] M. Tassopoulos and D. E. Rosner, Chem. Eng. Sci. **47**, 421 (1992).

[3] P. P. Mitra and P. N. Sen, Phys. Rev. B **45**, 143 (1992).

[4] P. P. Mitra, P. N. Sen, and L. M. Schwartz, Phys. Rev. B **47**, 8565 (1993).

[5] P. N. Sen, L. Schwartz, P. P. Mitra, and B. I. Halperin, Phys. Rev. B **49**, 215 (1994).

[6] V. N. Burganos, J. Chem. Phys. **109**, 6772 (1998).

[7] R. W. Mair, G. P. Wong, D. Hoffmann, M. D. Hurlimann, S. Patz, L. M. Schwartz, and R. L. Walsworth, Phys. Rev. Lett. **83**, 3324 (1999).

[8] M. D. Hurlimann, L. Venkataramanan, and C. Flaum, J. Chem. Phys. **117**, 10223 (2002).

[9] C. H. Arns, A. P. Sheppard, R. M. Sok, and M. A. Knackstedt, Petrophysics **48**(3), 202 (2007).

[10] D. S. Novikov and V. G. Kiselev, NMR Biomed. **23**, 682 (2010).

[11] L. H. Zheng and Y. C. Chiew, J. Chem. Phys. **90**, 322 (1989).

[12] S. Torquato and I. C. Kim, Appl. Phys. Lett. **55**, 1847 (1989).

[13] T. S. Ramakrishnan, L. M. Schwartz, E. J. Fordham, W. E. Kenyon, and D. J. Wilkinson, Petrophysics **40**(4), 260 (1999).

[14] C. H. Arns, T. Alghamdi, and Ji-Youn Arns, New J. Phys. **13**, 015004 (2011).

[15] M. A. Knackstedt, S. Latham, M. Madadi, A. Sheppard, T. Varslot, and C. Arns, The Leading Edge **28**, 28 (2009).

[16] S. Redner, *A Guide to First Passage Processes* (Cambridge University Press, Cambridge, UK, 2001).

[17] G. Picard and K. Frey, Phys. Rev. E **75**, 066311 (2007).

[18] E. Toumelin, C. T. Verdin, B. Sun, and K.-J. Dunn, J. Magn. Reson. **188**, 83 (2007).

[19] In many cases one is interested in the possibility of absorption when diffusing particles hit the solid interface. In that case the absorption strength translates into a probability that the walker will be annihilated at the grain boundary [3,5]. The issues addressed in this paper arise for any choice of boundary condition at the interface so we do not explicitly deal with absorption.

[20] In the reflection process the walker attemps to move from its initial position (in the pore space) into the solid grain. At the point where it hits the grain it reflects to its new position. The sum of the two distances traveled is equal to the step length ϵ.

[21] Our simulations are based on the granular models pictured in Figs. 5, 6, and 7. The value of ϵ is taken equal to the radius of the micrograins divided by 100.

[22] J. N. Roberts and L. M. Schwartz, Phys. Rev. B **31**, 5990 (1985).

[23] A. M. Chapman and J. J. L. Higdon, Phys. Fluids A **4**, 10 (1992) (see Table II).

[24] S. Ryu, Diffus. Fundam. **10**, 17.1 (2009); Special Issue "Magnetic Resonance in Porous Media" *A Selection of Papers Presented at the* 9th *International Bologna Conference Magnetic Resonance in Porous Media (MRPM 9), July 2008, Cambridge MA, USA* [http://www.uni-leipzig.de/diffusion/journal/contents_vol10.html].

[25] X. Zhan, L. M. Schwartz, M. N. Toksoz, W. C. Smith, and F. D. Morgan, Geophysics **75**, F135 (2010).

[26] P. J. McDonald, J.-P. Korb, J. Mitchell, and L. Monteilhet, Phys. Rev. E **72**, 011409 (2005).

[27] L. Monteilhet, J.-P. Korb, J. Mitchell, and P. J. McDonald, Phys. Rev. E **74**, 061404 (2006).

[28] M. Fleury and J. Soualem, J. Colloid Interface Sci. **336**, 250 (2009).

[29] C. H. Arns, K. E. Washburn, and P. T. Callaghan, Petrophysics **48**(5), 380 (2007).

[30] A. T. de Hoop and M. D. Prange, J. Phys. A **40**, 12463 (2007).

[31] M. Prange, V. Druskin, D. L. Johnson, and L. M. Schwartz, J. Phys. A: Math. Theor. **44**, 395203 (2011).